Dalton Transactions

Accepted Manuscript

ROYAL SOCIETY OF CHEMISTRY

www.rsc.org/dalton

Electron Transfer Rate Modulation in a Compact Re(I) Donor-Acceptor Complex

Yuankai Yue,[a] Tod Grusenmeyer,[a] Zheng Ma,[b] Peng Zhang,[b] Russell H. Schmehl,[a] David N. Beratan,[b] Igor V. Rubtsov[a] *

[a] *Department of Chemistry, Tulane University, New Orleans, Louisiana 70118;*

[b] *Departments of Chemistry, Biochemistry, and Physics, Duke University, Durham, North Carolina 27708*

irubtsov@tulane.edu

Abstract

Formation of the charge transfer state with the rate constant of $(10\ ps)^{-1}$ has recently been reported for the complex fac-[$Re^{I}(CO)_3$(DCEB)(3DMABN)] (ReEBA); where 3DMABN is 3-dimethylaminobenzonitrile, serving as an electron donor, and DCEB is 4,4'-(dicarboxyethyl)-2,2-bipyridine, serving as an electron acceptor (Y. Yue et all. *J. Phys. Chem. A*, **118**, 10407). 3-pulse UV-pump – IR-pump – IR-probe spectroscopy is used in this work to study how the charge separation reaction in ReEBA to form a ligand to ligand charge transfer state (LLCT) can be modulated by vibrational excitation of various modes of the complex. While no significant rate modulation was found when the cyano group stretching mode of the 3DMABN donor was excited, a sizable effect was found when the ring stretching mode of the DCEB acceptor was excited. The accumulation of the charge separated state (LLCT state) in the 3-pulse experiment was observed at a sharp excited-state vibrational peak of symmetric stretch of three facial carbonyl groups, ν_{SS}(CO). Modeling indicates that the rate of charge separation is increased by ca. 28% when vibrational excitation is present. The vibronic coupling signal of the bpy ring mode and ν_{SS}(CO) as well as the energy transport dynamics from bpy to carbonyl contributed to the 3-pulse signal and was studied as well using the 3-pulse method. The energy transport between the same modes, but in the ground electronic state, was measured by relaxation-assisted two-dimensional infrared (RA 2DIR) spectroscopy. The energy transport times of 4 ± 0.7 and 5 ± 1.5 ps were found for the ground and excited electronic states.

Key words: photoinduced charge transfer, electron transfer rate modulation, time-resolved infrared spectroscopy, relaxation-assisted 2DIR spectroscopy, transition-metal complexes

1. Introduction

Photoinduced electron transfer (PET) processes have been extensively studied for a variety of applications such as dye-sensitized solar cells, CO_2 reduction,[1] catalytic water oxidation and proton reduction.[2, 3] The control of the PET rate was often approached through structure modification on the molecular system of interest. Because of their well-defined structures and synthetically tunable excited state properties, rhenium complexes have been an excellent system for such studies.[4-9] Modification of one or more ligands can result in big differences in the excited state electron transfer properties. Beside the chemical modifications, optical modulation of the electron transfer (ElT) rate has also been demonstrated.[10,11] Mid-IR modulation of electron transfer rates is attractive, as it is chemically innocent, simple to control, and potentially mode specific. For systems with uniquely defined group vibrational modes, modulation of electron transfer rates following excitation of particular modes provides fundamental insight into the degree to which these modes are coupled to the electron transfer process.

The PET process in a donor-bridge-acceptor (DBA) assembly,[10] featuring guanosine-cytidine (GC) hydrogen-bonding bridge moiety, is found to be dependent on the presence of the vibrational excitation of the bridge vibrations. The mechanism of this modulation was proposed to be a weakening of the hydrogen bonding or distortion of the bridging π electron system by the vibrational excitation.

Modulation of the electron transfer rate between metal and the molecules adsorbed at the metal surface was reported.[12, 13] It is found that intramolecular vibrations of the molecules, such as NO and C_{140}, are strongly coupled to the electronic degrees of freedom, promoting the electron transfer reaction. Theoretical findings indicate that ElT kinetics can be changed by controlling the coherence of inelastic tunneling pathway interferences, creating a molecular analogue of the double-slit electron transmission experiment.[14-19] In systems with two interfering ElT coupling pathways, the excitation of a pathway-specific bridge vibration, which may induce electron-vibration energy exchange, labels the ET pathway and therefore modifies pathway interferences.[14-21] Here, we present another molecular system with the ElT rate tunable by the mid-IR radiation, in which the rate of charge separation is enhanced upon vibrational excitation.

Recently we reported a compact Re(I) compound (ReEBA, Scheme 1) that features fast photoinduced electron transfer with ca. 10 ps time constant between the 3DMABN and DECB

ligands,[5] where 3DMABN and DCEB denote 3-dimethylaminobenzonitrile and 4,4'-(dicarboxyethyl)-2,2'-bipyridine respectively. The charge separation process occurs as a transition from an initially formed triplet metal-to-ligand charge transfer (MLCT) excited state to a ligand-to-ligand charge transfer (LLCT) state; the LLCT state features almost a full-electron transfer from 3DMABN to DCEB. The ReEBA complex has several convenient IR modes that can be used either to track formation of the charge separated (LLCT) state or to pump in an attempt to modulate the ElT rate.

Scheme 1

We report the study of modulation of the rate of charge separation in ReEBA using 3-pulse UV-pump – IR-pump – IR-probe spectroscopy (Sections 3.1-3.3). Vibrational coupling of the mode excited by IR-pump, the tag mode, and the vibrational reporter is found to be contributing to the signals measured in the 3-pulse experiments, which makes the data analysis more complicated. In addition, vibrational energy transport from the tag mode to the reporter site contributes to the 3-pulse signals. Therefore, the energy transport process was carefully studied using the relaxation-assisted 2DIR spectroscopy (RA 2DIR, Section 3.4).[22] Kinetic modeling of the 3-pulse measurements is given in Section 3.5.

2. Experimental Details

2.1. UV-IR-IR 3-Pulse Transient Spectroscopy. Laser pulses at 804 nm generated by a Ti:sapphire oscillator were split into two parts to seed two regenerative amplifiers. The laser beam produced by one of the regenerative amplifiers (Spitfire Pro, Spectra-Physics) featuring pulses of 44 fs duration and 1.1 mJ energy at 1 kHz repetition rate was frequency doubled using a BBO crystal to generate 402 nm excitation pulses (ca. 1.5 μJ pulse energy was used in the experiments). This 402 nm excitation beam was delayed by a translation stage of 600 mm long (Parker) and focused into the sample cell using a 300 mm lens. The laser beam produced by the other regenerative amplifier (Legend, Coherent), which was synchronized with the Spitfire Pro amplifier, featuring pulses of 44 fs duration and 800 μJ energy at 1 kHz repetition rate was used to pump two in-house built optical parametric amplifiers (OPA), which produced signal and idler pairs. The signal-idler pairs were focused into 1.5 mm thick $AgGaS_2$ crystals, where two independently tunable mid-IR beams were generated through difference frequency generation process. Both mid-IR beams feature a spectral width of ca. 150 cm^{-1} and a pulse duration of ca.

120 fs. One of the mid-IR beams was delayed by a translation stage and used as a probe beam, while the other mid-IR beam served as a pump beam and was chopped at half the laser repetition rate. Both mid-IR beams were focused into the sample cell using a parabolic reflector. After passing through the sample cell, the IR probe beam was dispersed in a monochromator (Triax-190, HORIBA) and measured by a single channel MCT detector (MCT10-010-E-LN4, Electro-Optical System INC).

2.2. 2DIR and RA 2DIR Measurements. The details of a fully automated dual-frequency 3-pulse 2DIR instrument with heterodyned detection with the spectral range from 800 to 4000 cm^{-1} are presented elsewhere.[22] Briefly, a Ti:Sapphire laser, producing 1.5 W power at 1 kHz repetition rate, 800 nm wavelength, ca. 14 nm bandwidth (*fwhm*), and 80 fs pulse duration (Libra, Coherent), was used to pump a fully computer-controlled dual optical parametric amplifier (OPA, Palitra-duo, Quantronix). Two pairs of Signal and Idler OPA outputs were directed into two computer-controlled noncollinear difference-frequency generation (DFG) units (nIR-A and nIR-B, Quantronix), which generate mid-IR pulses with energies ranging from 1.5 to 10 μJ, depending on the central wavelength. The 2DIR instrument features separate schematics for stabilizing the directions of both mid-IR beams,[23] a unit to satisfy the phase matching conditions for the mid-IR beam directions at the sample, interferometric delay measurement units with active phase stabilization and phase modulation. The heterodyned signal is measured using a multi-channel MCT array detector (IR-6400, Infrared Associates) attached to a monochromator (Triax-190, HORIBA).

The 2DIR measurements were performed by scanning the delay between the first two pulses, τ, (both at the same central frequency) at a fixed waiting time, the delay between the second and third pulses, and recording the heterodyned spectrum in the frequency range of interest for every τ. Fourier transformation along the τ direction results in a 2DIR spectrum. About 2-4 min is required to measure a single 2DIR spectrum. For RA 2DIR measurements, the waiting time, *T*, was scanned and 2DIR spectra were recorded for each waiting time. It takes ca. 2 hours to measure typical waiting time dependence.

3. Results and Discussion

3.1. Selection of the Molecular System.

The ReEBA compound (Scheme 1) was selected for the study of the electron transfer rate modulation because it features fast charge separation rate and has a range of convenient vibrational modes (Fig. 1). Using a combination of transient infrared (UV-pump – IR-probe, TRIR) and transient absorption (UV-pump – vis-probe, TA) spectroscopies and DFT computations, it has recently been shown that an essentially full-electron ligand-to-ligand

Fig. 1

(3DMABN → DCEB) charge transfer (LLCT) state is formed in ReEBA upon excitation at 402 nm.[5] A triplet MLCT state formed within 200 fs after the excitation is accompanied by significant frequency shifts of many vibrational modes in the complex (Fig. 2). For example, the stretching modes of the 3 facial carbonyls (symmetric stretch at 2046 cm^{-1} and two asymmetric stretches appearing at ca. 1949 cm^{-1}) are known to be sensitive to the charge of the metal center due to back bonding.[24, 25] These modes shift to higher frequencies in the MLCT state, reflecting an increase in positive charge on the Re center, as apparent in the TRIR spectrum measured at 1 ps delay (Fig. 2). Small up-shift of the three carbonyl stretching modes is due to vibrational cooling in the MLCT state, which occurs with characteristic time of 17 ps.[4] The stretching mode of the cyano group appearing at 2258 cm^{-1} in the ground state is shifted to 2240 cm^{-1} in the MLCT state. The C=O stretching modes of the ester in the DCEB ligand, appearing at ca. 1735 cm^{-1}, is shifted to lower frequencies in the MLCT state by ca. 35 cm^{-1}, indicating an increased negative charge on the ligand. The ring stretching mode of the DCEB ligand (ν(bpy), 1610 cm^{-1}) is also shifted to lower frequencies by ca. 60 cm^{-1} and its IR intensity increases by ca. 10 fold. The experimental frequency shifts and DFT calculations indicate that the triplet MLCT state features a charge shift of about half of an electron from the Re center and the DCEB ligand,[5] which is similar to that found in other Re^{I} tricarbonyl complexes.[4]

Fig. 2

The MLCT state is converted to the LLCT state with a 10 ps characteristic time. The growth of ν_{SS}(CO) at 2023 cm^{-1} and ν_{AS}(CO) at 1910 and 1930 cm^{-1} and concomitant decay of the peaks at 2075, 1990, and 2240 cm^{-1} indicate the MLCT to LLCT conversion.[5] The ester carbonyl peak of the DCEB ligand (1700 cm^{-1}) is shifted further to lower frequencies by ca. 18 cm^{-1}, indicating an increase of a negative charge at the ester sites in the LLCT state. The DCEB ring stretching mode frequency (ca. 1540 cm^{-1}) changed little, but its IR intensity increases by ca. 18% in the LLCT state, suggesting that the negative charge at the bpy moiety changes little

between the two states. The ν_{SS}(CO) peak of the LLCT state found at 2023 cm^{-1} is very narrow and has a large extinction coefficient (7600 $M^{-1}cm^{-1}$); this makes it a good probe for detecting the amount of the LLCT states formed in the 3-pulse measurements.

3.2. Design of the 3-pulse Experiment.

The UV-IR-IR 3-pulse experiments use UV radiation at 402 nm to initiate the electron transfer process. After a delay time, t_1, an IR-pump pulse targeting specific spectral region is introduced to perturb the ElT process. The amount of the LLCT state formation is tested by the IR probe pulse as a function of the second time delay, t_2, between the IR pump and IR probe (Fig. 3). A vibrational band most sensitive to formation of the LLCT state should be selected for probing. As mentioned above, the symmetric stretch of the three facial carbonyl groups, ν_{SS}(CO), featuring in the LLCT state a narrow peak at 2023 cm^{-1} with a large extinction coefficient of 7600 $M^{-1}cm^{-1}$, is convenient for tracing the LLCT state formation (Fig. 2). Several vibrational modes were tested for their ability of modulating the ElT rate, including the CN stretching mode and ring stretching mode of the bpy located in the ground state at 2260 and 1610 cm^{-1}, respectively, but a sizable rate modulation is found only for the bpy ring mode excitation; these experiments are described in detail in this report. The IR pump pulse was centered at the peak at 1540 cm^{-1}, which belongs to the bpy stretching mode in the MLCT state (Fig. 2).

Fig. 3.

The 3-pulse transient spectra represent the difference between the transient IR spectra with and without the IR pump; they are recorded by optical chopping of the IR pump pulses at half the laser repetition rate. The 3-pulse transient spectra were measured at several t_2 delays and at two t_1 delays of 2 and 40 ps. At the small t_1 delay of 2 ps, the initially formed MLCT state still did not convert to the LLCT state and the ElT rate modulation by the IR pump can occur. On a contrary, at t_1 of 40 ps, which is much larger than the time constant of the LLCT state formation (10 ps), essentially all excited complexes are in the LLCT state and no rate modulation can be observed. Thus, by comparing the 3-pulse transient spectra and transient kinetics at t_1 = 2 ps and at 40 ps, the EIT modulation features can be identified. To map the kinetics of the LLCT state accumulation during t_2 delay time, the 3-pulse transient kinetics were measured at specific wavelengths characteristic for formation of the LLCT state (Fig. 4). Note that the rate modulation is observed cumulatively via observation of a different amount of the LLCT state

accumulated over some time interval. The IR-pump – IR-probe spectra have also been measured under the same experimental conditions as the 3-pulse spectra by blocking the UV excitation beam. The IR-pump – IR-probe spectra serve as a reference to help identify the IR-pump – IR-probe contributions to the 3-pulse signals.

Fig. 4.

3.3. Results of the 3-pulse Measurements

Figure 5A shows the 3-pulse transient spectrum (black) measured at small t_1 time delay of 2 ps and t_2 = 2 ps. Note that the IR pump spectrum was centered at 1540 cm^{-1}, while the IR probe was scanned between 1940 and 2080 cm^{-1}. For the t_1 delays much smaller than the MLCT→LLCT reaction time constant (10 ps), the MLCT state is the dominant excited state in the system. In addition, the transient spectrum measured at the same experimental conditions but with the UV pulses blocked, referred to as the IR-IR transient spectrum, is shown with a red line. Several spectral features can be assigned by comparing the two spectra. Because the bleach peak at 2050 cm^{-1} and the absorption peak at 2046 cm^{-1} are similar in both spectra, they do not require UV excitation and represent the 1600-1610 / CO_{SS} cross peak in the ground electronic state. The cross peak consists of the ground state bleach at $\nu_{SS}(CO)$ and absorption to the combination band of 1600-1610 modes and CO_{SS}, that is observed at $\nu_{SS}(CO) - \Delta_{1600/CO}$ frequency, where $\Delta_{1600/CO}$ is the off-diagonal anharmonicity of the two modes.

Fig. 5

The spectral features at 2023 and 2015 cm^{-1} are observed only in the 3-pulse spectra. The bleach at 2023 cm^{-1} matches the $\nu_{SS}(CO)$ peak in the LLCT state, observed in the TRIR measurements (Fig. 2); its appearance in the 3-pulse spectra can indicate the modulation of the rate of charge separation by the IR excitation. However, together with the negative peak at 2023 cm^{-1}, there is a positive peak at 2015 cm^{-1}; the appearance of the peak pair can be explained as the vibronic coupling signal of the bpy stretching mode (1540 cm^{-1}) and $\nu_{SS}(CO)$ (2023 cm^{-1}) in the LLCT state. The relation of the signal at 2023 cm^{-1} to the LLCT state is confirmed by the 3-pulse measurements where the t_2 delay is kept constant at 2 ps, while the t_1 time is scanned (Fig. 5B). The signal at 2023 cm^{-1} grows with the 8.4 ± 2 ps time constant indicating that it belongs to the LLCT state, as it matches well the rate of the charge separation (10 ± 1 ps).

The 3-pulse and IR-pump – IR-probe spectra were also measured at a larger t_1 time delay of 40 ps (not shown) and t_2 = 2 ps; at such t_1 values the majority (98%) of the MLCT states were converted to the LLCT state and no modulation of the ElT rate is possible. Similar peaks at 2023 and 2015 cm^{-1} were observed in these two measurements. The difference spectrum between the 3-pulse and IR-pump – IR-probe spectra measured at t_1 = 40 ps is shown in Fig. 5C. The best fit is shown with red line (see Fig. 5 caption).

While the peaks at 2023 and 2015 cm^{-1} are observed in the 3-pulse transient spectra at both small and large t_1 delays, the kinetic traces at 2023 cm^{-1} at small and large t_1 delays show dramatic differences (Fig. 6A). At t_1 = 40 ps, the kinetics at 2023 cm^{-1} shows an early time decrease with a maximum at ca. 6 ps; the signal then decays back to the baseline. However, at t_1 = 2 ps, the kinetics does not show any clear decrease at the early time, but also decays to the baseline. The data indicate that the t_1 = 2 ps kinetics has an additional contribution and since at t_1 = 40 ps no EIT modulation signal is expected, the difference between these two kinetic traces may be due the EIT rate modulation effect. The difference between the two kinetics (Fig. 6B) shows a rise followed by the decay, as expected for the ElT rate modulation dynamics (Fig. 4); its modeling is discussed in Section 3.5.

Fig. 6

3.4. Mode Coupling and Relaxation-assisted 2DIR Measurement.

The 3-pulse spectra clearly show signals that correspond to the vibrational coupling in the ground electronic and LLCT states. To better understand these contributions and to measure the coupling strength of the modes and energy transport dynamics between the ligands, relaxation-assisted 2DIR measurements were performed. The relaxation-assisted 2DIR (RA 2DIR) method relies on vibrational energy transport in molecules that originates from relaxation of the initially excited tag mode. Instead of the direct perturbation of the reporter mode frequency by excitation of the tag observed in traditional 2DIR, the RA 2DIR method relies on delivery of the excess energy introduced by the tag excitation to the region in the molecule where the reporter is located. The excited tag mode relaxes to other modes in the molecules and the excess energy is propagating along the molecular chain as a part of the energy dissipation process. Once it reaches the reporter mode site, the reporter mode frequency is perturbed and the cross-peak appears at the intersection of the tag and reporter mode frequencies. Cross peak enhancements as large as

27-fold were observed in the waiting time traces.[26] The RA 2DIR method provides an important new observable, the energy transport time, that can be a useful structural constraint.[27, 28] Due to through-bond connectivity observed for numerous molecules,[29-32] a smaller T_{max} values are found for the vibrational modes that are closer to the initially excited mode, permitting mode assignment based on the T_{max} values.

The relaxation-assisted 2DIR measurements were performed focusing on the cross peaks between the ν(bpy) and ν_{SS}(CO) modes. Figure 7 shows a 2DIR magnitude spectrum of ReEBA measured in the (1500 – 1700) / (1950 – 2070) cm^{-1} spectral region, featuring several cross peaks. A clear cross peak is observed at ca. 1605 / 2045 cm^{-1}. Because ν(bpy) is close in frequency to ν(ph) (1610 and 1600 cm^{-1}, respectively) their cross peaks with ν_{SS}(CO) are not spectrally resolved. However, the waiting-time dependences for these two cross peaks, plotted in Figure 8, have different T_{max} values, confirming that both ring modes are coupled to ν_{SS}(CO). The T_{max} values indicate the energy transport time from the excited vibrational mode, ν(bpy) or ν(ph), to the region where the probed mode is located. The T_{max} value for the ν(bpy) / ν_{SS}(CO) (3.5 ps) is smaller than that for the ν(ph) / ν_{SS}(CO) (5 ps), as the bpy is located closer to the metal carbonyls than the phenyl ring of 3DMABN. The kinetics of the ν(bpy) / ν_{SS}(CO) waiting time matches well the 3-pulse kinetic trace at 2023 cm^{-1}, measured at t_1 = 40 (Fig. 8, green line). The match indicates strongly that the 3-pulse kinetics vs. t_2 delay measured at t_1 = 40 ps at 2023 cm^{-1} originates from the ν(bpy) / ν_{SS}(CO) coupling in the LLCT state.

Fig. 7

Fig. 8

3.5. Data Analysis and Modeling.

A kinetics scheme used to model the experimental results is shown in Figure 4. The whole process is described as follows. The UV pulse excites ca. 5% of the complexes into the MLCT state, which converts into the LLCT state with a time constant k_1 of 10 ps. Introducing the IR excitation of the ring stretching mode of bpy (with ca. 3% excitation probability) results in an alternative reaction pathway that occurs from the vibrationally excited MLCT state, denoted as MLCT*. The respective rate constant, k_2, is the only tunable parameter in the scheme. The 3-pulse transient kinetic trace is modeled by taking the difference between the kinetics for these two paths, which represents the difference in the amount of LLCT state with and without IR

pump (see Fig. 6 caption). The best fit modeling kinetics is plotted in Figure 6B (red), together with the experimental data (blue). The rate constant (k_2) was varied and the best fit was found at $k_2 = (7.8\ \text{ps})^{-1}$ (Figure 6B). Note that the signal amplitude was the main parameter for the fit; the peak amplitude (in mOD) was referenced to the peak amplitude at 2023 cm^{-1} (also in mOD) measured in the UV-pump – IR-probe experiments (as in Fig. 2). The k_2 value obtained by matching the amplitude also reproduces well the time profile of the 3-pulse data. The modeling results indicate that the rate of the LLCT state formation is increased by 28% when the reaction proceeds from the vibrationally excited MLCT state.

Time-dependent DFT calculations using a B3LYP functional were carried out to map the potential energy surface of T2 (MLCT) and T1 (LLCT) triplet states in ReEBA. The energy difference between the T2 and T1 states along the two bpy stretching modes, 1544 cm^{-1} and 1576 cm^{-1} (both strongly IR active), computed at the equilibrium geometry of the T1 state, was monitored. The scan started from the T1 equilibrium structure and the results are presented in Figure 9. As one can see, the excitation of the bpy stretching modes will bring the two surfaces closer to near degeneracy point, resulting in a faster nonadiabatic electronic transition to from T2 to T1. Particularly, the mode of 1544 cm^{-1} is more effective in promoting the MLCT to LLTC transition. These results suggest that the bpy stretching modes are strongly coupled to the ElT reaction coordinate.

Concluding remarks

Several factors affected the data recorded in this study. One is related to degradation of the sample under UV radiation. Note that while the sample volume was substantial (>3 mL) and minimal overall degradation was observed after the experiments, the UV power had to be small to avoid precipitation on the optical windows. Even with the use of the flow cell the maximum power of the UV pump was rather low allowing to generate only less than 5% of excited molecules in the excited area of the sample. Lower UV power resulted in smaller 3-pulse signals. Another complication is associated with the presence of the vibrational and vibronic coupling signals, and the latter was masking the ElT modulation effect. In addition to vibronic coupling that is the strongest at zero time delay time between the IR pump and IR probe pulses, the energy transport dynamics originated from relaxation of the IR-pumped mode also contributed to the 3-pulse spectra and kinetics. Independent characterization of the energy transport performed using

the RA 2DIR method demonstrated that the transport dynamics is similar in the ground and excited states.[33] Comparison of the 3-pulse signals measured at small and large t_1 delays clearly shows an additional contribution attributed to the ElT modulation effect. Although the ElT modulation signals are not very large, the ElT rate change due to modulation is sizable (~28%), because of the small vibrational excitation probability (ca. 5%). Note that the bpy stretching mode, found to modulate the ElT rate, is capable of affecting the Re – bpy distance. It vibrational relaxation populates most likely other modes in the bpy which also can affect the Re-bpy coordination bonds. Because the short lifetime of the bpy stretching mode, the modes accepting energy from the initially excited bpy stretching mode are likely contributing to the modulation effect. The ElT time constant of 10 ps is too large to assess which specific mode is affecting the rate the most. Theoretical modeling demonstrates that bpy stretching modes are capable of modulating the ElT rate in ReEBA; more involved calculations are ongoing and will be reported elsewhere.

Acknowledgement. Support by the National Science Foundation (CHE-1012371 to I.V.R. and CHE- 012357 to D.N.B.) and the U.S. Department of Energy, Office of Chemical Sciences (DE-FG-02-96ER14617 to R.H.S.) is gratefully acknowledged. The Louisiana Board of Regents (Grant LEQSF(2011-12)-ENH-TR-29) is thanked for supporting acquisition of the fs Ti:Sapphire laser system. T.G. wishes to thank the Louisiana Board of Regents for Graduate Fellowship support. Y.Y. is thankful for a fellowship from the IBM Corporation.

Figures

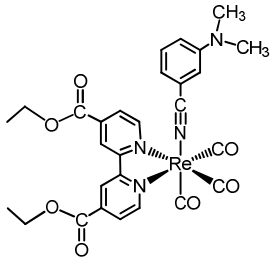

Scheme 1. Structure of the $Re^{I}(CO)_3$(DCEB)(3DMABN) compound, referred to as ReEBA.

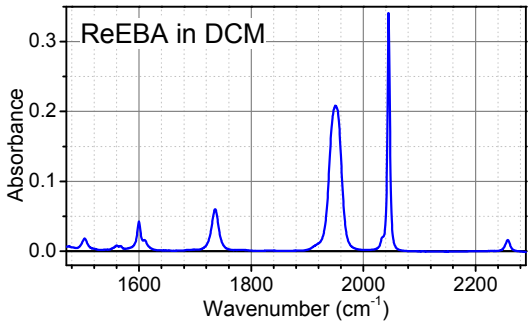

Fig. 1. Linear FTIR absorption spectrum of ReEBA in DCM measured at 9 mM concentration in the sample cell with 50 μm path length.

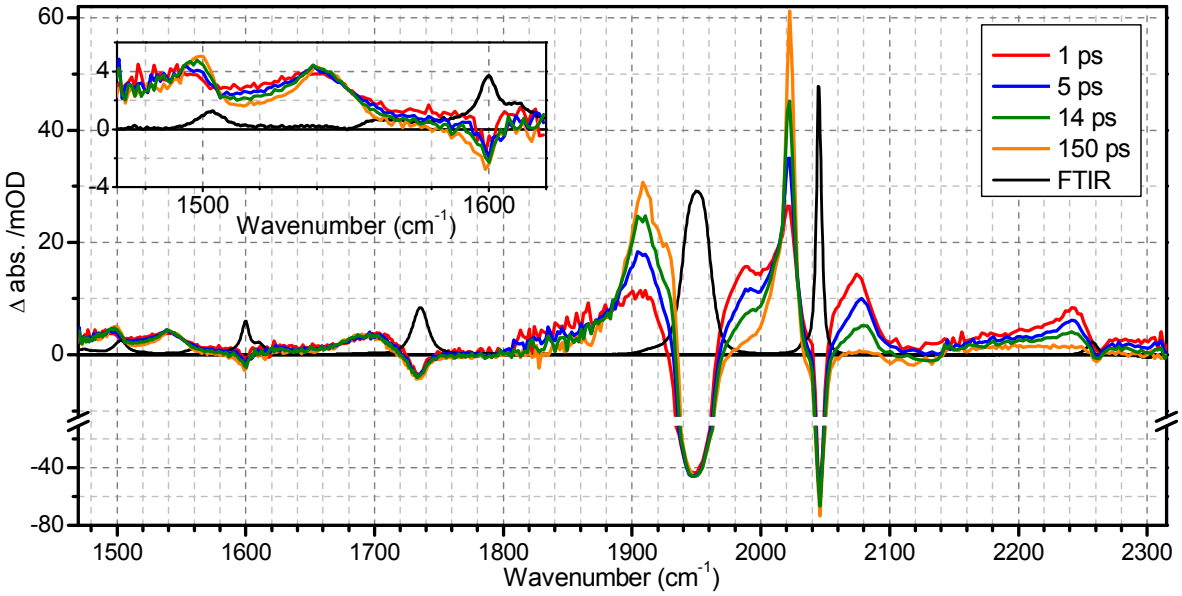

Fig. 2. Transient infrared spectrum of ReEBA in DCM at selected time delays (see inset) following the 402 nm excitation. The inset shows enlarged spectra at ring stretching region.

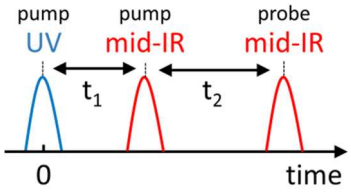

Fig. 3. Pulse sequence used in the 3-pulse experiments.

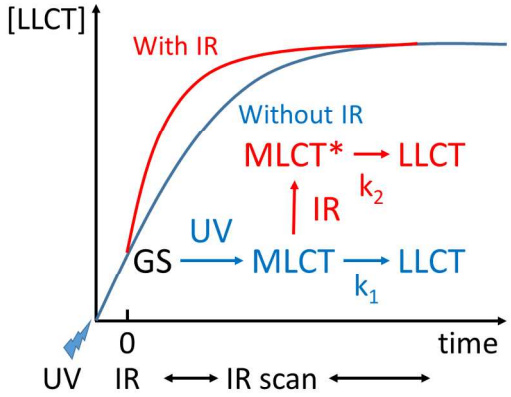

Fig. 4. Schematic representation of the expectations in the 3-pulse experiments. Dynamics of the LLCT state formation without (blue curve) and with (red curve) IR pump are shown, assuming that the ElT rate increases with IR pump.

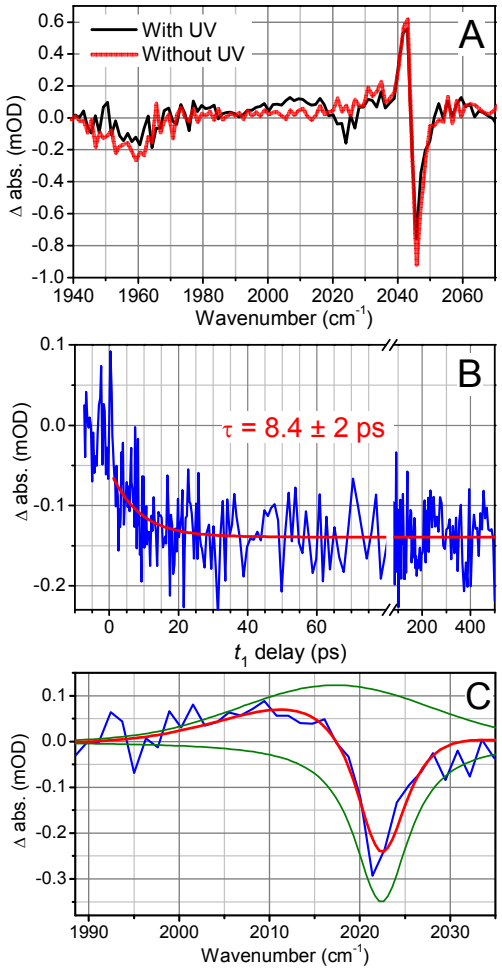

Fig. 5. **A.** 3-pulse and IR-pump – IR-probe transient spectra of ReEBA at t_1 = 2 ps, t_2 = 2 ps, both measured at the same experimental conditions. **B.** Transient 3-pulse kinetics measured at 2023 cm^{-1} and t_2 = 2 ps. The red curve shows the fit with a single exponential function. **C.** The difference between 3-pulse and IR-pump – IR-probe transient spectra measured at t_1 = 40 ps, t_2 = 2 ps and its fit (red) using the Lorentzian profile for the bleach peak with the width of 7.4 cm^{-1} (fwhm) that matches the peak at 2022.4 cm^{-1} in Fig. 2, and Gaussian profile for the transient absorption peak centered at 2017.3 cm^{-1} with the width of 24 cm^{-1} matching the peak at 1540 cm^{-1}. The bleach and absorption components are shown with green lines. The IR excitation frequency in the measurements was 1540 cm^{-1}.

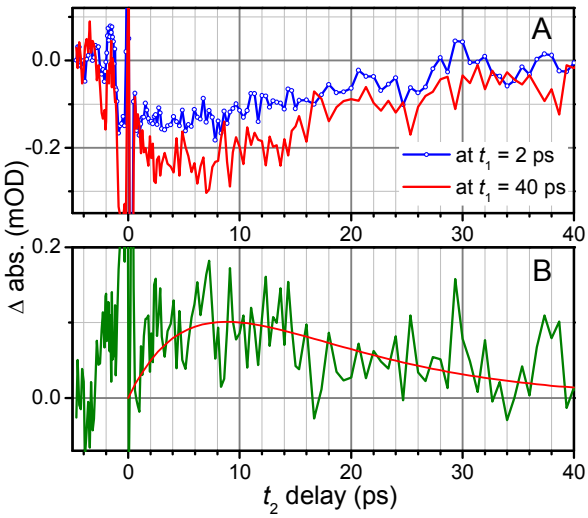

Fig. 6. A. The 3-pulse t_2 kinetics measured at 2023 cm^{-1} at two t_1 delays: 2 ps (blue) and 40 ps (red). A normalization factor of 1.2 was applied to the kinetics curve at t_1 = 40 ps to match the values at t_2 close to zero with those of the kinetics at t_1 = 2 ps. **B.** The difference (green) between the two kinetics shown in panel A. The red curve represents the modeling, with the equation $S(t_2) = A\,exp(-k_1 t_1) \times QY[\exp(-k_1 t_2) - \exp(-k_2 t_2)]$ where QY denotes the vibrational excitation probability (MLCT*/MLCT), evaluated to be 3% and A is the maximum of the LLCT peak at 2023 cm^{-1} (in mOD) formed under the actual conditions of both 2-pulse and 3-pulse experiments. The k_1 rate constant of (10 ps)$^{-1}$ was used in the modeling. The k_2 value of (7.8 ps)$^{-1}$ was obtained from the fit.

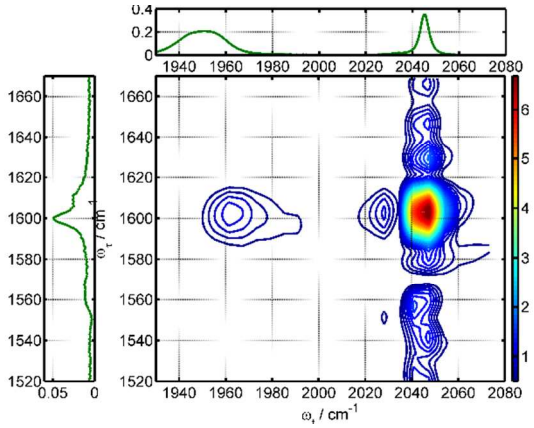

Fig. 7. 2DIR spectrum of ReEBA in DCM measured at 3 ps waiting time. The first two excitation pulses were centered at 1600 cm^{-1} and the third pulse and the local oscillator were centered at 2040 cm^{-1}. The linear spectrum of ReEBA is shown in the attached panels.

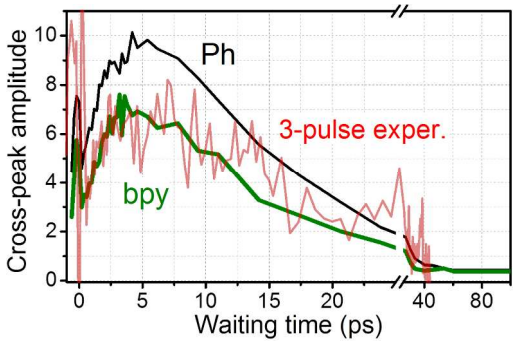

Fig. 8. Waiting-time dependences of the and ν(bpy)/ν_{SS}(CO) (green) and ν(ph)/ν_{SS}(CO) (black) cross peaks in the ground electronic state measured via RA 2DIR. The IR pulses, the first two and the third, were centered at 1600 and 2040 cm^{-1}, respectively. The normalized 3-pulse t_2 kinetics measured at 2023 cm^{-1} at 40 ps delay (red curve in Fig. 6A) is shown for comparison.

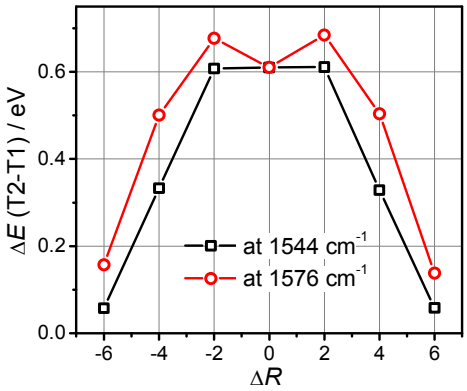

Fig. 9. Potential energy difference (in eV) between the T1 and T2 states computed along the bpy stretching normal coordinates for the modes at 1544 cm^{-1} (black) and 1576 cm^{-1} (red). ΔR is the relative displacement of the equilibrium geometry along the normal mode (ΔR=0 corresponds to the T1 state equilibrium structure).

References

1. H. Takeda and O. Ishitani, *Coord. Chem. Rev.*, 2010, **254**, 346-354.
2. O. V. Prezhdo, W. R. Duncan and V. V. Prezhdo, *Acc. Chem. Res.*, 2008, **41**, 339-348.
3. M. D. Karkas, E. V. Johnston, O. Verho and B. Akermark, *Acc. Chem. Res.*, 2014, **47**, 100-111.
4. Y. Yue, T. Grusenmeyer, Z. Ma, P. Zhang, T. T. Pham, J. T. Mague, J. P. Donahue, R. H. Schmehl, D. N. Beratan and I. V. Rubtsov, *J. Phys. Chem. B*, 2013, **117**, 15903-15916.
5. Y. Yue, T. Grusenmeyer, Z. Ma, P. Zhang, R. H. Schmehl, D. N. Beratan and I. V. Rubtsov, *J. Phys. Chem. A*, 2014, **118**, 10407-10415.
6. S. Verma, P. Kar, A. Das and H. N. Ghosh, *Dalton Trans.*, 2011, **40**, 9765-9773.
7. J. D. Lewis, M. Towrie and J. N. Moore, *J. Phys. Chem. A*, 2008, **112**, 3852-3864.
8. M. Busby, A. Gabrielsson, P. Matousek, M. Towrie, A. J. Di Bilio, H. B. Gray and A. Vlcek, Jr., *Inorg. Chem.*, 2004, **43**, 4994-5002.
9. M. Delor, I. V. Sazanovich, M. Towrie, S. J. Spall, T. Keane, A. J. Blake, C. Wilson, A. J. Meijer and J. A. Weinstein, *J. Phys. Chem. B*, 2014, **118**, 11781-11791.
10. Z. Lin, C. M. Lawrence, D. Xiao, V. V. Kireev, S. S. Skourtis, J. L. Sessler, D. N. Beratan and I. V. Rubtsov, *J. Am. Chem. Soc.*, 2009, **131**, 18060-18062.
11. M. Delor, P. Scattergood, I. Sazanovich, M. Towrie, G. M. Greetham, A. W. Parker and J. A. Weinstein, 245th ACS National Meeting & Exposition, New Orleans, LA, United States, 2013.
12. M. Silva, R. Jongma, R. W. Field and A. M. Wodtke, *Annu. Rev. Phys. Chem.*, 2001, **52**, 811-852.
13. A. N. Pasupathy, J. Park, C. Chang, A. V. Soldatov, S. Lebedkin, R. C. Bialczak, J. E. Grose, L. A. Donev, J. P. Sethna, D. C. Ralph and P. L. McEuen, *Nano Lett.*, 2005, **5**, 203-207.
14. D. Xiao, S. S. Skourtis, I. V. Rubtsov and D. N. Beratan, *Nano Lett.*, 2009, **9**, 1818-1823.
15. D. N. Beratan, S. S. Skourtis, I. A. Balabin, A. Balaeff, S. Keinan, R. Venkatramani and D. Xiao, *Acc. Chem. Res.*, 2009, **42**, 1669-1678.
16. S. S. Skourtis, D. H. Waldeck and D. N. Beratan, *The Journal of Physical Chemistry B*, 2004, **108**, 15511-15518.
17. M. D. Newton, *Int. J. Quantum Chem.*, 2000, **77**, 255-263.
18. H. B. Gray and J. R. Winkler, *Q. Rev. Biophys.*, 2003, **36**, 341-372.
19. E. S. Medvedev and A. A. Stuchebrukhov, *The Journal of Chemical Physics*, 1997, **107**, 3821.
20. H. Carias, D. N. Beratan and S. S. Skourtis, *J. Phys. Chem. B*, 2011, **115**, 5510-5518.
21. S. S. Skourtis, D. H. Waldeck and D. N. Beratan, *Annu. Rev. Phys. Chem.*, 2010, **61**, 461-485.
22. J. D. Leger, C. M. Nyby, C. Varner, J. Tang, N. I. Rubtsova, Y. Yue, V. V. Kireev, V. D. Burtsev, L. N. Qasim, G. I. Rubtsov and I. V. Rubtsov, *Rev. Sci. Instrum.*, 2014, **85**, 083109.
23. C. M. Nyby, J. D. Leger, J. Tang, C. Varner, V. V. Kireev and I. V. Rubtsov, *Opt Express*, 2014, **22**, 6801-6809.
24. C. J. Kleverlaan, D. J. Stufkens, I. P. Clark, M. W. George, J. J. Turner, D. M. Martino, H. van Willigen and A. Vlček, *J. Am. Chem. Soc.*, 1998, **120**, 10871-10879.
25. D. J. Liard, M. Busby, P. Matousek, M. Towrie and A. Vlček, *J. Phys. Chem. A*, 2004, **108**, 2363-2369.
26. V. M. Kasyanenko, Z. Lin, G. I. Rubtsov, J. P. Donahue and I. V. Rubtsov, *J. Chem. Phys.*, 2009, **131**, 154508/154501-154508/154512.
27. V. M. Kasyanenko, S. L. Tesar, G. I. Rubtsov, A. L. Burin and I. V. Rubtsov, *J. Phys. Chem. B*, 2011, **115**, 11063-11073.
28. C. S. Keating, B. A. McClure, J. J. Rack and I. V. Rubtsov, *J. Phys. Chem. C*, 2010, **114**, 16740-16745.

29. D. V. Kurochkin, S. G. Naraharisetty and I. V. Rubtsov, in *Springer Series in Chemical Physics*, eds. P. Corkum, D. M. Jonas, R. J. D. Miller and A. M. Weiner, Springer, 2007, vol. 88, pp. 344-346.
30. D. V. Kurochkin, S. R. Naraharisetty and I. V. Rubtsov, *Proc. Natl. Acad. Sci. U. S. A.*, 2007, **104**, 14209-14214.
31. I. V. Rubtsov, *Acc. Chem. Res.*, 2009, **42**, 1385-1394.
32. H. M. Muller-Werkmeister, Y. L. Li, E. B. Lerch, D. Bigourd and J. Bredenbeck, *Angew Chem Int Ed Engl*, 2013, **52**, 6214-6217.
33. E. H. G. Backus, P. H. Nguyen, V. Botan, R. Pfister, A. Moretto, M. Crisma, C. Toniolo, G. Stock and P. Hamm, *J. Phys. Chem.*, 2008, **112**, 9091-9099.